FROM NUCLEAR FORCES AND EFFECTIVE FIELD THEORY TO NUCLEAR STRUCTURE AND REACTIONS*

Dean Lee

Facility for Rare Isotope Beams and Department of Physics and Astronomy
Michigan State University, East Lansing, MI 48824, USA

(Received November 16, 2018)

We discuss several recent developments connecting the fundamental theory of the strong interactions and bare nuclear forces to nuclear structure and reactions. In particular, we review recent results in the area of nuclear lattice simulations based on chiral effective field theory by the Nuclear Lattice EFT Collaboration. The topics we cover are lattice interactions with improved rotational properties, nuclear physics near a quantum phase transition, seeing nuclear structure through pinholes, and a computational method called eigenvector continuation.

DOI:10.5506/APhysPolB.50.253

1. Introduction

There have been many recent developments connecting the fundamental theory of the strong interactions and bare nuclear forces to the structure and dynamics of atomic nuclei. There are several collaborations that use lattice quantum chromodynamics (QCD) to probe nucleon–nucleon interactions from first principles [1–3]. There has also been progress in computing reactions such as proton fusion and triton decay [4]. Meanwhile, there have been numerous recent developments on nuclear structure and reactions starting from the bare nuclear forces and the framework of chiral effective field theory [5–7].

Chiral effective field theory (EFT) describes the low-energy interactions of nucleons. It consists of an expansion in powers of momenta and factors of the pion mass near the chiral limit, where the light quarks are massless. See Ref. [8] for a review of chiral EFT. Terms with a total of n powers of nucleon

* Presented at the Zakopane Conference on Nuclear Physics "Extremes of the Nuclear Landscape", Zakopane, Poland, August 26–September 2, 2018.

momenta or factors of the pion masses are labelled as order Q^n. The leading order (LO) interactions are at order Q^0, the next-to-leading order (NLO) interactions correspond to order Q^2, next-to-next-to-leading order (N2LO) terms are Q^3, and next-to-next-to-next-to-leading order (N3LO) are Q^4. In this proceedings article, we review several recent results using chiral EFT by the Nuclear Lattice EFT Collaboration.

2. Improved lattice interactions

Nuclear lattice simulations using chiral EFT have been used to describe the structure and scattering of atomic nuclei [9–11]. However, the treatment of nuclear forces at higher orders in the chiral expansion are difficult on the lattice due to the breaking of rotational invariance produced by the nonzero lattice spacing [12, 13].

In Ref. [14], we solve these problems with a new set of short-range chiral EFT interactions on the lattice that decomposes more easily into spin channels. The key idea is to define smeared annihilation and creation operators. This procedure gives us simpler rotational symmetry properties when taking spatial derivatives as finite differences. We start with $a_{i,j}(\boldsymbol{n})$, the nucleonic annihilation operator on lattice site $\boldsymbol{n}$ with spin i and isospin j. To this, we add neighboring lattice operators with relative weight, $s_{\rm NL}$, to define the smeared annihilation operator

$$a_{i,j}^{s_{\rm NL}}(\boldsymbol{n}) = a_{i,j}(\boldsymbol{n}) + s_{\rm NL} \sum_{|\boldsymbol{n}'|=1} a_{i,j}\left(\boldsymbol{n}+\boldsymbol{n}'\right) . \tag{1}$$

Next, we form bilinear functions of the annihilation operators with various spin and isospin quantum numbers, S, S_z, I, I_z,

$$\left[a(\boldsymbol{n})a\left(\boldsymbol{n}'\right)\right]_{S,S_z,I,I_z}^{s_{\rm NL}} = \sum_{i,j,i',j'} a_{i,j}^{s_{\rm NL}}(\boldsymbol{n}) M_{ii'}(S,S_z) M_{jj'}(I,I_z) a_{i',j'}^{s_{\rm NL}}\left(\boldsymbol{n}'\right) . \tag{2}$$

We introduce orbital angular momentum using solid spherical harmonics

$$R_{L,L_z}(\boldsymbol{r}) = \sqrt{\frac{4\pi}{2L+1}} r^L Y_{L,L_z}(\theta,\phi) , \tag{3}$$

that are written as functions of the lattice derivatives acting on one of the annihilation operators

$$P_{S,S_z,L,L_z,I,I_z}^{2M,s_{\rm NL}}(\boldsymbol{n}) = \left[a(\boldsymbol{n})\boldsymbol{\nabla}_{1/2}^{2M} R_{L,L_z}^*(\boldsymbol{\nabla}) a(\boldsymbol{n})\right]_{S,S_z,I,I_z}^{s_{\rm NL}} . \tag{4}$$

We then project onto the selected spin and orbital angular momentum using Clebsch–Gordan coefficients

$$O^{2M,s_{\rm NL}}_{S,L,J,J_z,I,I_z}(\boldsymbol{n}) = \sum_{S_z,L_z} \langle SS_zLL_z|JJ_z\rangle P^{2M,s_{\rm NL}}_{S,S_z,L,L_z,I,I_z}(\boldsymbol{n})\,. \tag{5}$$

In Ref. [14], we present results for the neutron–proton system up to N3LO for lattice spacings of 1.97, 1.64, 1.32, and 0.99 fm. In Fig. 1, we show results for the neutron–proton scattering phase shifts and mixing angles *versus* the relative momenta for lattice spacing $a = 0.99$ fm. The blue, green and red bands signify the estimated uncertainties at NLO, N2LO and N3LO, respectively. The black solid lines denote phase shifts or mixing angles from the Nijmegen partial wave analysis and the diamonds indicate lattice results at N3LO.

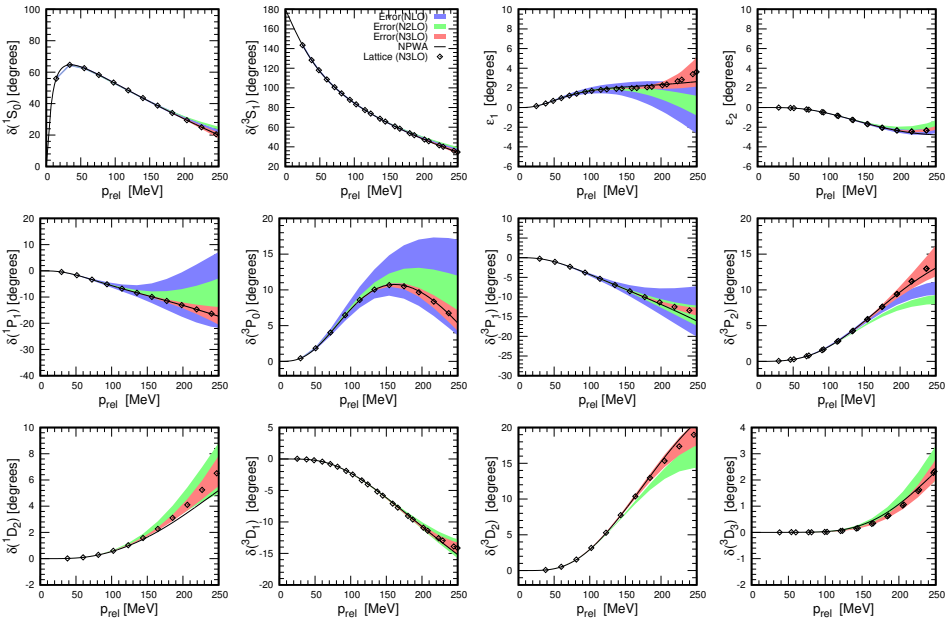

Fig. 1. (Color online) Results for the neutron–proton scattering phase shifts and mixing angles *versus* the relative momenta for lattice spacing $a = 0.99$ fm.

3. Nuclear physics near a quantum phase transition

In Ref. [15], we consider two LO interactions, A and B, at lattice spacing $a = 1.97$ fm that have nearly the same nucleon–nucleon phase shifts and nearly the same similar three- and four-nucleon bound state properties. However, the binding energies for larger nuclei are found to be quite different. In Table I, we show results for the ground state energies of ^{8}Be, ^{12}C, ^{16}O, and ^{20}Ne using interactions A and B at LO with Coulomb interactions and the comparison with experimental data. We see that while the ground state energies for B track rather well with experimental data, the ground state energies for A are significantly underbound. In order to identify the source of the problem, we consider the ground state energies of ^{8}Be, ^{12}C, ^{16}O, and ^{20}Ne for interaction A without Coulomb interactions. When we compute the ratio of the Coulomb-free ground state energies to the Coulomb-free ^{4}He ground state energy, we find the ratios

$$\frac{E_{^{8}\mathrm{Be}}}{E_{^{4}\mathrm{He}}} = 1.997(6)\,, \quad \frac{E_{^{12}\mathrm{C}}}{E_{^{4}\mathrm{He}}} = 3.00(1)\,, \quad \frac{E_{^{16}\mathrm{O}}}{E_{^{4}\mathrm{He}}} = 4.00(2)\,, \quad \frac{E_{^{20}\mathrm{Ne}}}{E_{^{4}\mathrm{He}}} = 5.03(3)\,. \tag{6}$$

The simple integer values are consistent with the formation of a Bose condensate of alpha particles filling the periodic box. In Ref. [15], we provide further evidence that this interpretation is correct by showing that the alpha–alpha interactions are almost negligible for interaction A.

TABLE I

Results for the ground energies of ^{8}Be, ^{12}C, ^{16}O, and ^{20}Ne using interactions A and B at LO with Coulomb interactions and the comparison with experimental data.

Nucleus	A (LO + Coulomb)	B (LO + Coulomb)	Experiment
^{8}Be	−56.51(14)	−57.29(7)	−56.591
^{12}C	−84.0(3)	−89.9(5)	−92.162
^{16}O	−110.5(6)	−126.0(7)	−127.619
^{20}Ne	−137(1)	−164(1)	−160.645

Hence, we have numerical evidence that nature is near a quantum phase transition. For even and equal numbers of protons and neutrons, there is a first-order transition at zero temperature from a Bose-condensed gas of alpha particles to a nuclear liquid. Whether one has a Bose gas of alpha particles or a nuclear liquid is determined by the strength of the alpha–alpha interactions. Meanwhile, the alpha–alpha interactions are sensitive to the strength of the local part of the nucleon–nucleon interactions. The local part of the interactions is much stronger for interaction B as compared with interaction A. By local, we mean interactions that are velocity-independent.

In Fig. 2, we show the zero-temperature phase diagram of nuclear matter. λ indicates the strength of the local part of the interactions. For λ below the critical value, nuclear matter is in a Bose gas phase of alpha particles. For λ above the critical value, nuclear matter is in a nuclear liquid phase. As λ increases further, finite A-body nuclei become stable relative to their corresponding multi-alpha thresholds at energies $E_\alpha A/4$.

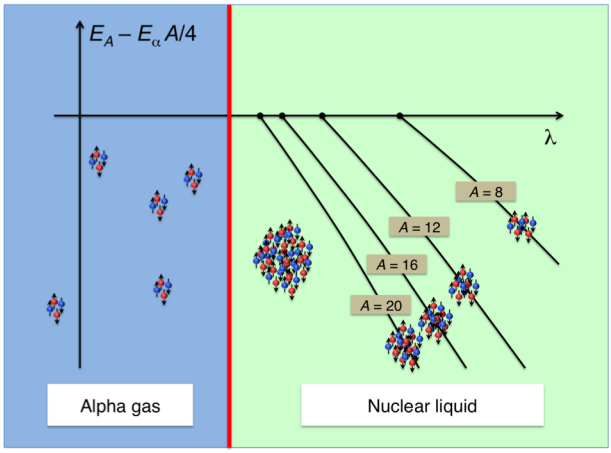

Fig. 2. Zero-temperature phase diagram of nuclear matter. λ indicates the strength of the local part of the interactions.

4. Seeing nuclear structure with pinholes

The Nuclear Lattice EFT Collaboration uses auxiliary fields to perform Monte Carlo simulations. In Ref. [16], we introduce a new approach called the pinhole algorithm that overcomes computational problems in auxiliary-field Monte Carlo simulations when computing density correlations relative to the center of mass. For a nucleus with A nucleons, the pinhole algorithm consists of computing expectation values of the normal-ordered A-body density operator

$$\rho_{i_1,j_1,\ldots,i_A,j_A}(\boldsymbol{n}_1,\ldots,\boldsymbol{n}_A) = :\rho_{i_1,j_1}(\boldsymbol{n}_1)\ldots\rho_{i_A,j_A}(\boldsymbol{n}_A):\ . \tag{7}$$

In addition to updating the auxiliary field configurations, we also perform Monte Carlo updates of the pinhole positions $\boldsymbol{n}_1,\ldots,\boldsymbol{n}_A$ and pinhole indices $i_1,j_1,\ldots,i_A,j_A$. We note the simple sum rule that summing over all pinhole positions and indices yields $A!$ times the identity operator.

The pinhole algorithm gives us the positions of the nucleon as a classical distribution. Using the pinhole algorithm, we have computed the proton and neutron densities for the ground states of ^{12}C, ^{14}C, and ^{16}C. The results are

shown in Fig. 3 along with the experimentally observed proton densities. From Fig. 3, we see that the agreement between the calculated proton densities and experimental data for ^{12}C and ^{14}C [17] is rather good. We show data for $L_t = 7, 9, 11, 13, 15$ time steps. In these calculations, we have used a spatial lattice spacing of 1.97 fm and lattice time spacing 1.97 fm/c. The fact that the results have almost independent of L_t means that we are measuring ground state properties. As the number of neutrons increases, going

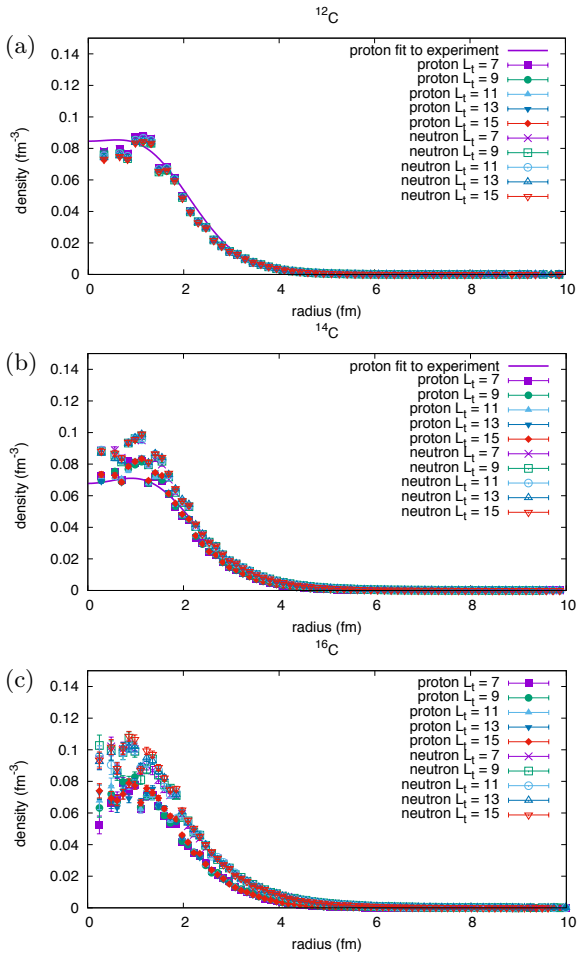

Fig. 3. Plots of the proton and neutron densities for the ground states of ^{12}C, ^{14}C, and ^{16}C *versus* radial distance. We show data for $L_t = 7, 9, 11, 13, 15$ time steps. We show ^{12}C in panel (a), ^{14}C in panel (b), and ^{16}C in panel (c). The errors are one-standard deviation error bars associated with the stochastic errors. For comparison, we show the experimentally observed proton densities for ^{12}C and ^{14}C [17].

from ^{12}C to ^{16}C, the shape of the proton density profile remains roughly the same. We note that the excess neutrons in ^{14}C and ^{16}C are distributed fairly evenly, appearing in both the central region as well as the tail.

5. Eigenvector continuation

In nuclear theory and other fields of quantum theory, we often would like to find the extremal eigenvalues and eigenvectors of a Hamiltonian matrix in a vector space that is extremely large, so large that linear algebra operations on general vectors cannot be performed. Monte Carlo methods are well-suited to overcome this problem, however, stochastic methods fail when severe sign oscillations appear and there is strong cancellation between positive and negative amplitudes.

In Ref. [18], we present a new technique called eigenvector continuation (EC) that can improve the reach of Monte Carlo methods. The main idea is that while an eigenvector inhabits a linear space with very many dimensions, the eigenvector trajectory generated by smooth changes of the Hamiltonian matrix can be well-approximated by a low-dimensional manifold. This statement is proven using analytic continuation.

Suppose that the Hamiltonian $H(c)$ depends smoothly on some control parameter c. Let $c_\odot$ be the target value of the parameter for which we wish to compute the ground state wave function $|\Psi_0(c_\odot)\rangle$. The EC method is a variational calculation where the variational subspace consists of eigenvectors $|\Psi_0(c)\rangle$ for different values of c. In Ref. [18], we consider simulations of the neutron matter at leading order using the lattice action described in Ref. [19]. This particular lattice action is plagued by large sign oscillations due to the one-pion exchange interaction, which is parameterized by the coupling g_A^2. The systems we calculate are the ground state energies of 6 and 14 neutrons on a $4 \times 4 \times 4$ lattice with spatial lattice spacing of 1.97 fm and time lattice spacing of 1.32 fm. We first attempt to compute the ground state energies by direct calculation. The errors are quite large due to sign oscillations. For 6 neutrons, the ground state energy is $E_0 = 12(^{+3}_{-4})$ MeV, and for 14 neutrons, $E_0 = 42(^{+7}_{-15})$ MeV.

Next, we use eigenvector continuation for values $g_A^2 = c_1, c_2, c_3$, where $c_1 = 0.25$, $c_2 = 0.60$, and $c_3 = 0.95$. We use Monte Carlo simulations to calculate the ground state eigenvectors for c_1, c_2, c_3. In Table II, we show the EC results using just one of the three vectors, two of the vectors, or all three vectors. The error bars are estimates of the stochastic error and extrapolation error in projection time. For comparison, we also show the direct calculation results. The EC results are consistent with the direct calculation results, though with an error bar that is smaller by an order of magnitude. Eigenvector continuation approach is now being developed for all interactions that produce sign oscillations in the nuclear lattice simulations.

TABLE II

Eigenvector continuation results for the ground state energy for six and fourteen neutrons using sampling data $g_A^2 = c_1, c_2, c_3$, where $c_1 = 0.25$, $c_2 = 0.60$, and $c_3 = 0.95$. For comparison, we also show the direct calculation results.

g_A^2 values	E_0, 6 neutrons [MeV]	E_0, 14 neutrons [MeV]
c_1	14.0(4)	48.8(6)
c_2	13.7(4)	48.5(7)
c_3	13.8(6)	48.8(8)
c_2, c_3	13.7(4)	48.4(7)
c_3, c_1	13.8(4)	48.8(6)
c_1, c_2	13.7(4)	48.4(7)
c_1, c_2, c_3	13.7(4)	48.4(7)
Direct calculation	$12\,(^{+3}_{-4})$	$42\,(^{+7}_{-15})$

REFERENCES

[1] M.L. Wagman *et al.*, *Phys. Rev. D* **96**, 114510 (2017).

[2] T. Iritani *et al.*, *Phys. Rev. D* **96**, 034521 (2017).

[3] E. Berkowitz *et al.*, *Phys. Lett. B* **765**, 285 (2017).

[4] M.J. Savage *et al.*, *Phys. Rev. Lett.* **119**, 062002 (2017).

[5] T.D. Morris *et al.*, *Phys. Rev. Lett.* **120**, 152503 (2018).

[6] V. Lapoux *et al.*, *Phys. Rev. Lett.* **117**, 052501 (2016).

[7] E. Gebrerufael, K. Vobig, H. Hergert, R. Roth, *Phys. Rev. Lett.* **118**, 152503 (2017).

[8] E. Epelbaum, H.W. Hammer, U.-G. Meißner, *Rev. Mod. Phys.* **81**, 1773 (2009).

[9] E. Epelbaum, H. Krebs, D. Lee, U.-G. Meißner, *Phys. Rev. Lett.* **106**, 192501 (2011).

[10] E. Epelbaum *et al.*, *Phys. Rev. Lett.* **109**, 252501 (2012).

[11] S. Elhatisari *et al.*, *Nature* **528**, 111 (2015).

[12] J.M. Alarcón *et al.*, *Eur. Phys. J. A* **53**, 83 (2017).

[13] N. Klein *et al.*, *Eur. Phys. J. A* **54**, 121 (2018).

[14] N. Li *et al.*, *Phys. Rev. C* **98**, 044002 (2018).

[15] S. Elhatisari *et al.*, *Phys. Rev. Lett.* **117**, 132501 (2016).

[16] S. Elhatisari *et al.*, *Phys. Rev. Lett.* **119**, 222505 (2017).

[17] F.J. Kline *et al.*, *Nucl. Phys. A* **209**, 381 (1973).

[18] D. Frame *et al.*, *Phys. Rev. Lett.* **121**, 032501 (2018).

[19] D. Lee, *Lect. Notes Phys.* **936**, 237 (2017).